Submitted to *KONA: Powder and Particle* 1997-06-01. Revised 1997-08-15.

Measuring Slugging Bed Dynamics with Acoustic Sensors

C.E.A. Finney
University of Tennessee
Knoxville TN 37996-2210 USA

C.S. Daw
Oak Ridge National Laboratory
Oak Ridge TN 37831-8087 USA

J.S. Halow
Federal Energy Technology Center
Morgantown WV 26507-0880 USA

Abstract

We describe experimental observations of slugging bed dynamics with passive acoustic sensors. Our results indicate that acoustic signals contain both similar and complementary information relative to dynamic pressure signals. We find that selective preprocessing of acoustic signals is a key step in separating information about microscale and macroscale processes. With such preprocessing, both linear and nonlinear dynamical features are apparent. Nonlinear features appear to be especially useful for practical diagnostics.

1. Introduction

In many commercial and research applications of fluidized beds, dynamic pressure measurements are routinely employed to assess the quality and/or regime of fluidization. While such measurements are extremely useful, they present several engineering difficulties, including tap penetration of the vessel wall, plugging of the taps by particulates, and modulation of the dynamic signal by lines connecting the taps and pressure sensors. These difficulties provide an incentive to develop other options for making dynamic measurements, especially in cases where installation of pressure taps is constrained by severe process conditions or cost (*e.g.*, pressurized fluidized-bed combustion).

We selected acoustic measurements for study because of our qualitative observation that audible sound changes correlate with fluidization state. In particular, rhythmic "whooshing" sounds associated with rising bubbles seem to be a characteristic feature of many fluidized beds. Acoustic measurements are also attractive from the standpoint that they can be completely nonintrusive and are not subject to erosion, corrosion, or plugging. Although we found we could clearly distinguish fluidization states in laboratory beds by ear, an inspection of the raw acoustic signals showed them to be highly complex with a broad frequency spectrum. Thus it appears that the human ear does some rather sophisticated processing of the raw bed sounds.

From the results of this study we demonstrate that, at least in some cases, it is possible quantitatively to distinguish fluidization states by analyzing passive acoustic signals from the bed. Further, we show that acoustic signals can provide an alternative source of fluidization information which can be used to complement or even replace dynamic pressure measurements. Our working hypothesis is that acoustic signals from fluidized beds contain information about both microscale events (*e.g.*, particle-particle and particle-wall collisions) and macroscale events (*e.g.*, bubbles, global bed motion). The degree to which useful fluidization diagnostics can be developed depends upon the ability to separate these two different types of information.

In the following discussion, we illustrate signal processing techniques that work well for beds with large particles operating in a slugging or near-slugging mode. Our technique allows us to determine physical bubble/slug features and nonlinear dynamical (*i.e.*, chaotic) features which are important to bed performance and scale-up.

2. Background

Many different measurement systems have been used to monitor fluidized-bed dynamics (*i.e.*, observe the time evolution of the bed or its parts), ranging from sophisticated three-dimensional x-ray and capacitance imaging to optical and conductivity probes to flush, wall-mounted pressure taps. Example descriptions of many of these techniques are given in Clark *et al.* [1], Clift and Grace [2], Fan [3], Geldart [4], and Kühn *et al.* [5], and reviews are given by Yates and Simons [6] and Chaouki *et al.* [7].

Recent studies of the nonlinear and chaotic nature of fluidized beds have focused primarily on high-speed pressure measurements because they are relatively easy to make (at least in the laboratory) and they are commonly available on commercial beds. It is also believed that, at least in bubbling beds, pressure measurements strongly reflect the bubble patterns that dominate heat and mass transfer. Skrzycke *et al.* [8], Hay *et al.* [9], Schouten *et al.* [10], vander Stappen [11], and Karamavruç and Clark [12] illustrate

implementations of dynamic pressure measurements and analysis for bubbling or slugging beds.

Studies of acoustic measurements such as that by Cody *et al.* [13] have focused primarily on microscale dynamics; specifically, on the "random" component of particle motion associated with the granular temperature. In contrast, we are primarily interested in obtaining information about larger-scale dynamic phenomena such as bubbles and slugs.

We specifically want to use acoustic signals collected externally either through the bed wall or from the surrounding air to make inferences about fluidization quality. There are a number of practical problems associated with interpreting such signals, among which are attenuation or modulation of the sound by the bed wall and surroundings, background noise (*e.g.*, from gas flow or building vibrations), and distinguishing features associated with large-scale, collective solids motion from small-scale individual particle motion.

In order to start with a well-defined problem, we ran our experiments with ambient-temperature, transparent beds of large particles (*i.e.*, particles in Geldart groups D and B). Our objective was to explore the potential for extracting information from bed sounds that would be useful for diagnostics and possibly control. In the discussion below, we do not mean to imply that our results can be extended generally to all beds. Rather, we propose that our basic concepts for sound processing are likely to be suited for slugging conditions with Group D or B particles.

3. Experimental apparatus and procedure

In this study we investigated three different bed sizes and five different particulate solids. The first fluidized bed consisted of a 7.6-cm-diameter by 68-cm-long acrylic tube equipped with a perforated-plate grid. The grid contained 185 0.15-cm-diameter holes. Air was drawn through the bed by an acoustically insulated blower. Various materials, including an ellipsoidal crisp rice cereal with spherical equivalent diameter of 0.58 cm and density of 0.107 gm/cc, millet seed with equivalent diameter of 0.35 cm and density of 0.97 gm/cc, and corn (maize) with equivalent diameter of 0.91 cm and density of 1.25 gm/cc, were fluidized in the bed. Settled bed heights ranged from 15 to 45 cm. Sounds from the bed were captured by a directional microphone, then bandpass filtered (1600–6300 Hz) through a graphic equalizer and recorded with a DAT recorder at 44.1 kHz. After the experiment, the recorded sounds were processed by passing them to a computer sound card and digitizing at 22.05 kHz.

The second fluidized bed consisted of a 10.2-cm-diameter by 260-cm-long plexiglass tube. Regulated pressurized air from the building compressor was introduced into the plenum, where the air passed through seven tuyeres into the bed. The bed material was uniform 0.45-cm-diameter steel spheres with material density of 7.5 gm/cc, and the static bed height was 23.5 cm. The sound system was an analog sound-level meter, and the meter output signal was recorded, as-measured or bandpass filtered (0.1–6 Hz), with a 12-bit digitizing oscilloscope (Nicolet 440) at 200 Hz. The meter was set to a fast response rate with an "A" weighting, which integrated the acoustic intensities between 0.5 and 10 kHz, and was mounted horizontally 2.5 cm from the bed wall 17.5 cm above the grid. Additionally, a Baratron differential pressure transducer measured the pressure drop between taps located 10 and 23 cm above the distributor. The pressure signal was bandpass filtered (0.1–20 Hz) and recorded with the digitizing oscilloscope at 200 Hz.

The third fluidized bed was a 15.9-cm-diameter by 280-cm-long plexiglass tube with a similar air supply system as the 10.2 cm bed. The bed material was polyethylene powder between 0.25 and 1.0 mm diameter (0.63 mm mean diameter) with a particle density of 0.83 gm/cc, and the static bed height was 31.8 cm. Based on size and density, these particles are classified as Geldart Group B. The sound system was a piezoelectric acoustic pickup (model AGT 100 from Engineered Products Marketing Ltd. of St. Thomas, Ontario, Canada), which is commercially produced for the amplification of acoustic guitars. The output from the pickup was bandpass filtered (0.1–20 Hz) and recorded with the digitizing oscilloscope at 200 Hz. Additionally, a Baratron differential pressure transducer measured the pressure drop between taps located 18.5 and 28.5 cm above the distributor, and the pickup was mounted on the outside bed wall 23.5 cm above the distributor between the two pressure taps. The transducer signal was bandpass filtered (0.1–40 Hz) and recorded with the digitizing oscilloscope at 200 Hz.

The filter settings for the latter two beds were chosen to enhance signal features associated with bubble and slug events, which were expected to be primarily concentrated in frequencies less than 30 Hz [8]. Such filtering also reduces 60-Hz contamination from nearby AC power systems and prevents signal aliasing.

For all three beds, we recorded between 20 and 300 seconds of sound from each bed after it was fully

fluidized. As bubbles or slugs approached the surface, they expanded the solids locally and caused the surface to rise. Particle-particle or particle bed wall collisions during this expansion, rise and subsequent collapse appear to be the source of the "whooshing" sound captured in the recordings. With the 7.6-cm bed system, there was significant background noise from the nearby blower and other sources, whereas the 10.2- and 15.9-cm bed systems were relatively free of background noise.

4. Results

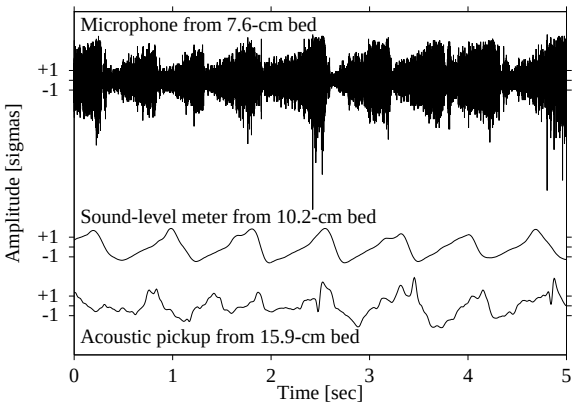

Fig. 1 Segments of typical acoustic-sensor measurements. Notice the predominant longer-timescale (0.5—1.0 sec) oscillations or modulations in all time series.

4.1 General features of our acoustic signals

Figure 1 illustrates typical acoustic time series from the three different measurement systems. The microphone time series from the 7.6-cm bed contains much high-frequency information, but the low-frequency amplitude modulation appears to reflect bubbles. The time series from the 10.2- and 15.9-cm beds appear less complicated, partly because of the nature of the instrumentation and partly because of signal preprocessing. The time series from all three measurements exhibit longer timescale (0.5 to 1.0 sec) dynamics corresponding with slugging and overall bed motion. Thus, one expects that an appropriate filter could emphasize either small- or large-scale dynamics, depending on the cutoff frequency.

4.2 Slugging patterns

The general fluidization behavior that we observed followed patterns described in Daw *et al.* [14] and M'chirgui *et al.* [15]. Specifically, we observed a transition from defluidized solids to turbulent fluidization as gas velocity was increased. For gas flows slightly above the *minimum fluidization velocity*, U_{mf}, particles near the bed surface vibrate but experience no net translation. The layer of vibrating particles deepens with increasing flow rate, but the movement still occurs at spatial scales on the order of 1—2 particle diameters. Pressure differential measurements across the layer of vibrating particles suggest complex dynamics involving a large number of inter-particle collisions, but these fluctuations are very small relative to those in the slugging regime.

With further increase in gas flow, macroscopic motion begins in the form of gas bubbles. The bubbling regime for Group D particles occurs only over a narrow flow range and changes abruptly to slugging at higher flow, whereas the bubbling regime for Group B particles occurs over a wider flow range before slugging occurs. In slugging, each rising bubble spans nearly the entire cross section of the bed and pushes a large mass of particles in front of it. We refer to each set of upward-moving particles as a *solid slug*, and the gas pocket is referred to as a *slug*. Particles move downward through and around the rising slug until it reaches the top of the bed, whereupon a settled bed is re-established, and the cycle repeats.

As the fluidizing velocity approaches a critical value, slugging becomes nearly periodic and appears to be very regular. We refer to this condition as *maximum stable slugging* and to the critical gas flow as the *maximum stability flow*, U_{mss} [14]. As flow increases beyond U_{mss}, the slugging amplitude increases and the time interval between slugs becomes more irregular. This irregularity occurs in the form of intermittent "stutters" in the otherwise periodic slugging pattern. Eventually, as the gas flow reaches a significant fraction of the terminal flow, fluidization approaches the turbulent regime.

4.3 Slugging diagnostics

For steel particles in the 10.2-cm bed, acoustic and pressure data were recorded at three fluidization conditions. **Figure 2** displays representative time-series segments of the acoustic and pressure measurements at flows of U/U_{mf} of 1.3, 1.4 and 1.7. The time series in these plots have been normalized to have unit standard deviation. From this figure, it is apparent that the acoustic and pressure signals provide complementary information, although there is a visible phase difference. This phase difference is actual and not an artifact of the

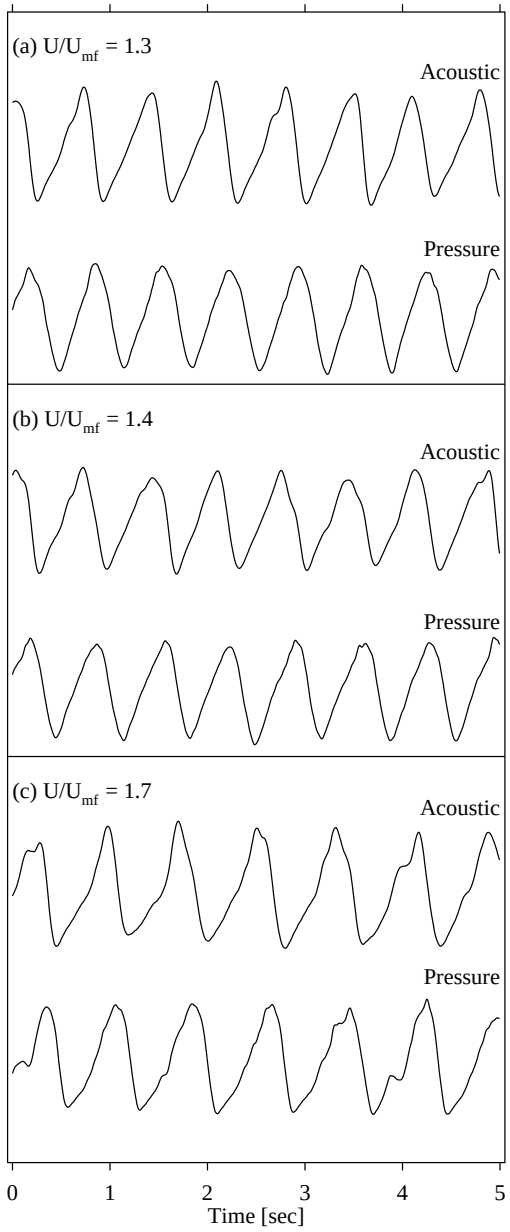

Fig. 2 Filtered sound-meter and pressure time series from the 10.2-cm bed at three different fluidization conditions.

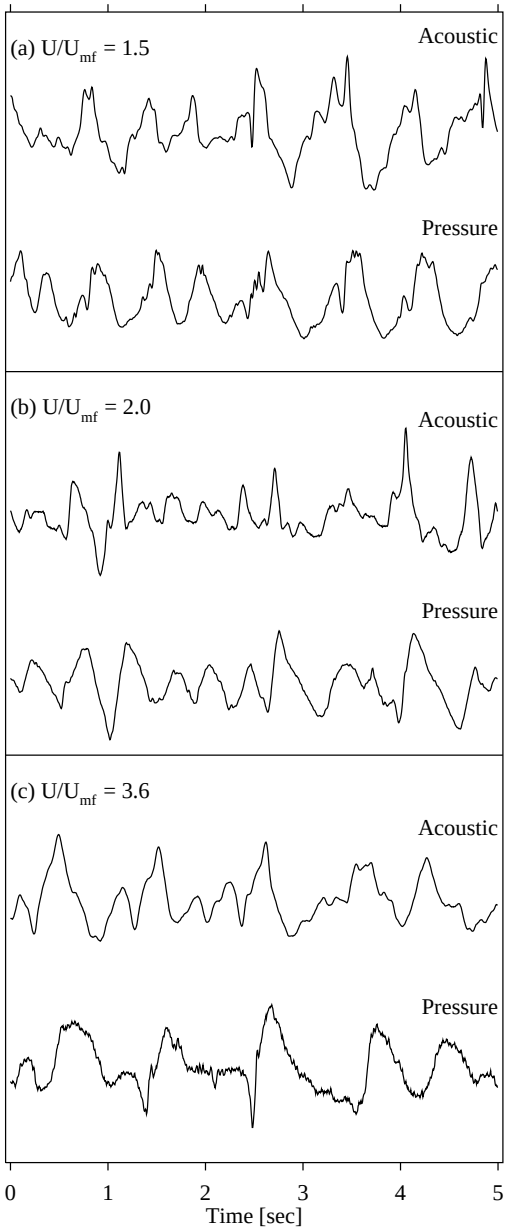

Fig. 3 Filtered acoustic-pickup and pressure time series from the 15.9-cm bed at three different fluidization conditions.

lowpass filtering. The fluidization states for U/U_{mf} values of 1.3 and 1.4 are fairly regular and very similar, whereas that at U/U_{mf} of 1.7 is less regular and rather different than the other two states.

For polyethylene particles in the 15.9-cm bed, acoustic-pickup and pressure data were recorded at three fluidization conditions. **Figure 3** displays representative time-series segments of the acoustic and pressure measurements at flows of U/U_{mf} of 1.5, 2.0 and 3.6. The acoustic pickup appears to detect vibrations along the wall corresponding to the disturbance of particles caused by a bubble passage. However, the maximal vibratory disturbance occurs when the bubble has passed through the bed and the solids collapse, as the acoustic

signal precedes peaks in the pressure signal with sharp peaks. At the highest flow condition (**Figure 3(c)**), the bed is slugging and vibrating very vigorously, so the acoustic signal, lowpass filtered at 20 Hz, appears fairly noisy. The figure displays the acoustic signal lowpass filtered at 4 Hz, which helps to highlight large-scale features as seen in the simultaneously measured pressure signal. Thus, for sharp changes in the pressure signal, corresponding large peaks in the acoustic signal are visible.

4.4 Physical interpretation of acoustic signals

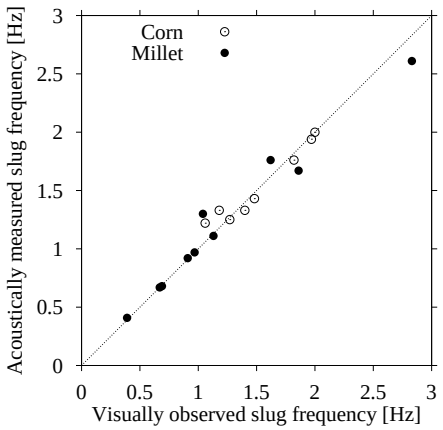

Fig. 4 Correlation between visually observed and acoustically measured slugging frequencies.

It is evident from **Figures 2–3** that acoustic signals correlate fairly well with pressure signals. Visual observation of a slugging bed in the acrylic tubes also indicates a correlation of sound with slug motion and that most of the sound comes from the particles flowing around or falling through the slug. To demonstrate this correlation, slugging frequencies were measured in the 7.6-cm bed by both visual observation and by recording and counting the acoustical pulses. The measurements were made with several materials over a range of fluidization velocities. **Figure 4** shows the strong correlation between the visually and acoustically determined slug frequencies (see [25]). The deviations were cases in which small bubbles were present and there was some uncertainty, either visually or acoustically, in determining whether a bubble was actually present.

Taking the impact of particles falling around or through slugs as the principal sound source, we can estimate the relationship between acoustic measurements and physical parameters. We assume particles free fall and accelerate prior to impact. The kinetic energy of a particle at impact equals its potential energy at the start of its fall:

$$K.E. = m_p\, g\, L_{slug} \qquad \textbf{(1)}$$

where m_p is the mass of the particle, g is the acceleration of gravity and L_{slug} is the length of the slug.

The rate of impacts can be related to the slug rise velocity. For the slug to rise, an equal volume of solids must flow around or fall through the slug. Multiplying this volumetric flow rate by the bulk density gives the mass flow rate:

$$\textit{Mass flow rate of particles} = \rho_{mf}\, U_{slug}\, A_{tube} \qquad \textbf{(2)}$$

where ρ_{mf} is the density of the solids at minimum fluidization, U_{slug} is the rise velocity of the slug, and A_{tube} is the cross-sectional area of the tube. The number of particles falling per second equals the mass rate divided by the mass of a single particle. The rate of total kinetic energy released from the impact of falling particles is:

$$\textit{Total rate of K.E.} = g\, \rho_{mf}\, A_{tube}\, L_{slug}\, U_{slug} \qquad \textbf{(3)}$$

Only a fraction, α, of the total kinetic energy will be converted to acoustic energy, transmitted through the wall, and captured by the microphone and recorded. The slug rise velocity is proportional to the square root of the slug length [16]. Substituting for the slug velocity, including the α, and collecting the constant terms into a parameter Z gives:

$$\textit{Rate of acoustic energy recorded} = Z\, L_{slug}^{3/2} \qquad \textbf{(4)}$$

where

$$Z = \alpha\, g\, \rho_{mf}\, A_{tube} \sqrt{\frac{g}{2+\left(\frac{A^*}{1-A^*}\right)^2}} \qquad \textbf{(5)}$$

A^* is the ratio of the slug cross-section to the bed cross-sectional area. In round-nosed slugs this is usually

about 0.75 and in wall slugs about 0.82.

Slugs form in fluidized beds by coalescence of small bubbles released at the grid. They continue to grow as long as any bubbles remain within about two bed diameters of them. During the growth period, the slug length is increasing and therefore the acoustic intensity will increase. A reasonable assumption for the rate of growth is that the slug collects all of the gas in excess of minimum fluidization velocity, so the slug length increases linearly with time. The acoustic intensity therefore increases with time to the 3/2 power. Once the stable size has been reached, the slug length will remain constant and the acoustic intensity will remain constant.

Because the acoustic energy is released during discrete impact events, the signal consists of numerous spikes superimposed on a background noise signal. The energy release in each impact may vary depending on the exact angle between the centers of the impacting particles. Essentially the parameter α varies with each impact. The raggedness in the microphone signal in **Figure 1** illustrates this point. An integral of the RMS value of the acoustic signal over the duration of the passage of a slug through the bed can be used to smooth out these impacts and variations. We divide the slug history into a growth period ending in t_{growth}. This period is followed by a stable non-growing period which ends when the slug reaches the surface at $t_{surface}$. With these definitions, the integral of the RMS becomes:

$$Integral\ RMS = Z(U-U_{mf})^{3/2}\frac{2}{5}t_{growth}^{5/2} + ZL_{slug}^{3/2}(t_{surface}-t_{growth}) \quad \textbf{(6)}$$

where U is the bed superficial velocity.

Figure 5 presents the integral RMS signal for slugs in a fluidized bed. The experiments were performed in the 7.6-cm bed with millet seed, fluidized at 110 cm/sec. Each point is derived from the signal for an individual slug. Most slugs appear reasonably similar in size and velocity with a relatively small number of small bubbles. The upper line in the figure has a slope of 1, illustrating the linear relationship of the RMS integral with duration for stable slugs. The lower line with a slope of 2.5 is what would be expected for slugs during their growth stage. The data in this region show more scatter, probably because there are fewer impacts being averaged for each signal. However, the trends seem to be consistently above the 2.5 sloped line,

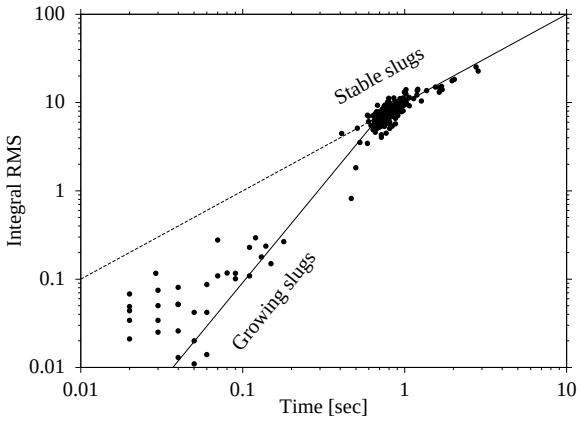

Fig. 5 Audio signal dependence on time. Lines represent expected behaviors based on **Eq. 6**.

indicating some less-sensitive dependence. Data from other velocities and bed conditions give similar results. The figure suggests that the basic interpretation of the origin of acoustic signals is correct, but more experimental work is needed to generalize these results.

4.5 Linear and nonlinear dynamical features

We employ three widely used time-series statistics for characterizing the recorded signals: power spectral density function, mutual information and Kolmogorov entropy.

We use a standard FFT-based power spectral density (PSD) function estimator to describe the frequency content of recorded signals. Similar PSDs between simultaneously measured acoustic and pressure signals should help to demonstrate that acoustic measurements contain similar and complementary frequency information to pressure measurements. As noted recently by other researchers, PSDs are of limited usefulness for characterizing fluidized beds because they assume an underlying linear structure in the signal[17,18]. This assumption does not hold when strong nonlinearities are present, and the resulting spectra can be inadequate to distinguish significantly different fluidization states.

The mutual information function [19] has become a standard tool in nonlinear signal processing, and the bivariate mutual information function has been demonstrated as a useful tool to measure coupling between simultaneously measured signals in fluidized beds [20,21]. Mutual information measures the amount

of predictability of a test signal as a function of time based on a reference signal. Given two simultaneous measured time series, *R* for reference and *T* for test, the average mutual information of a future or past measurement T_{i+k} with respect to present measurement R_i is

$$I(R_i \mid T_{i+k}) = H(R_i) + H(T_{i+k}) - H(R_i \mid T_{i+k}) \quad \textbf{(7)}$$

where *H(R)* and *H(T)* are unconditional entropies of measurements *R* and *T* and $H(R \mid T)$ is the conditional entropy of *T* given *R*, and *k* is the delay. Entropy takes the form

$$H(X) = -\sum p(X_j) \log p(X_j) \quad \textbf{(8)}$$

where *p(X)* represents the binned probability of event *X*, where *j* is summed over all bins. For base-2 logarithms, *H* and *I* are expressed in bits.

Large values of mutual information denotes strong coupling between the signals. When *k* is allowed to range from negative values to positive values, the average phase differences between the signals are highlighted. For a peak in *I* for time series *T* with respect to *R*, for $k<0$ certain events in *T* are said to "lead" those in *R*, whereas for $k>0$ certain events in *T* and said to "lag" those in *R*. For physical systems in which measurement errors or unstable dynamics are present, the amount of mutual information is expected to decrease as the delay increases.

Kolmogorov entropy quantifies the amount of information loss in a signal, and we use a form of the maximum-likelihood estimator of Kolmogorov entropy (K_{ml}) by Takens [22]. The K_{ml} has been proved to be a reliable standard measure of fluidized-bed pressure signals [10,11]. As described by Schouten *et al.* [22], it is necessary to specify an appropriate embedding window and an upper lengthscale for determining maximum-norm separations between trajectory segments (*i.e.*, points on the embedded trajectory). We use the term "entropy spectrum" to describe the values in K_{ml} when either the embedding window or the upper lengthscale is varied and the other parameter is held constant [23].

A useful measure based on the maximum-likelihood Kolmogorov entropy is to normalize the entropy value with respect to the entropy value taken from a randomized time series with the same probability distribution as the test time series. This "normalized entropy" thus ranges in value from 0 (purely periodic and infinitely predictable) to 1 (purely random and unpredictable).

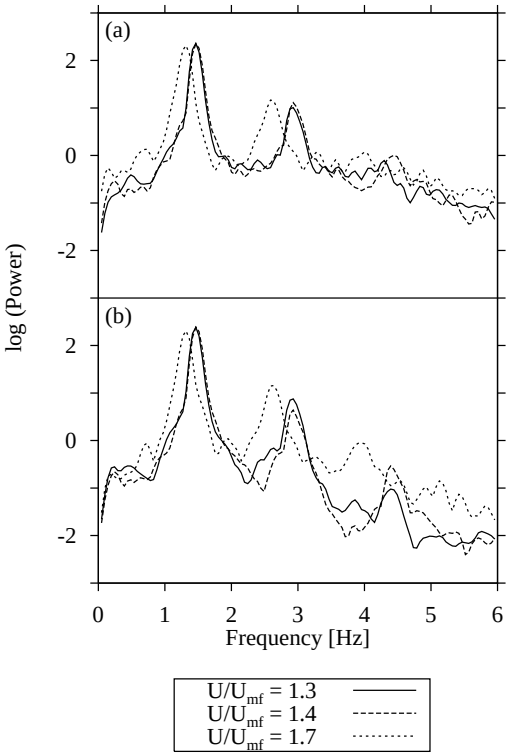

Fig. 6 PSDs for acoustic (a) and pressure (b) signals from the 10.2-cm bed at three fluidization conditions.

Figure 6 shows PSDs for the acoustic and pressure signals at three fluidization conditions in the 10.2-cm bed. With both signals, the PSDs for U/U_{mf} of 1.3 and 1.4 are very similar and dissimilar to those for U/U_{mf} of 1.7. The differences between the U/U_{mf} of 1.3 and 1.4 PSDs are most visible in the 0—1 and 4—5 Hz ranges in the acoustic signal and beyond 2 Hz in the pressure signal, and differences at other frequencies are hard to distinguish as either being real dynamical differences or artifacts of the PSD construction (limited, nonstationary data). However, the acoustic and pressure signals share similar content in the major peaks which represent the dominant slugging frequencies. Nevertheless, it is difficult to distinguish signals at U/U_{mf} of 1.3 and 1.4 using only the PSDs and to assign a statistical confidence to degrees of difference.

We present two types of entropy spectra. In the first type, the embedding window is held constant to a value equal to the average orbital time (defined as the

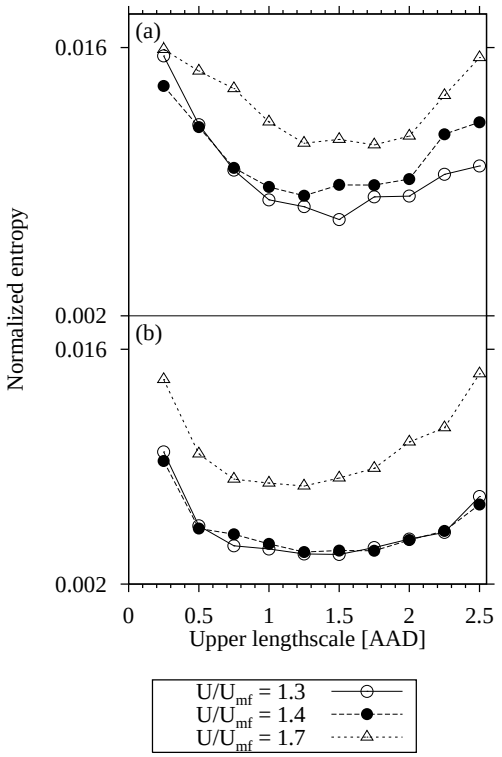

Fig. 7 Normalized entropy-lengthscale spectra for acoustic (a) and pressure (b) signals from the 10.2-cm bed at three fluidization conditions.

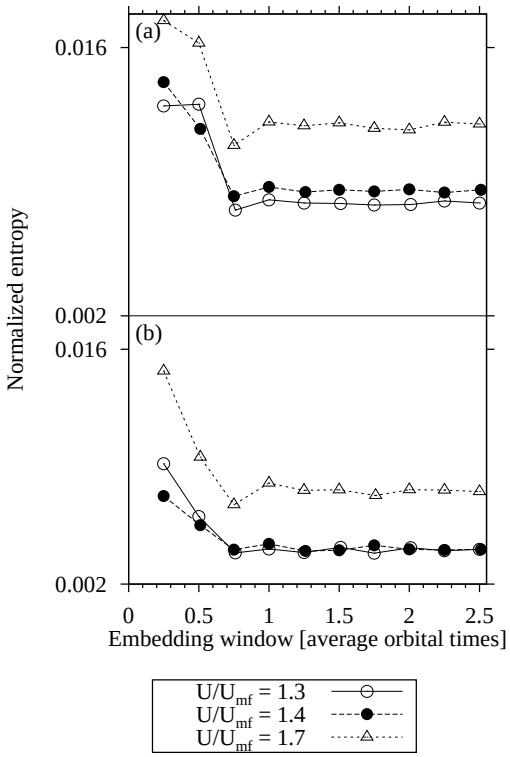

Fig. 8 Normalized entropy-timescale spectra for acoustic (a) and pressure (b) signals from the 10.2-cm bed at three fluidization conditions.

average number of measurement timesteps between successive up-crossings of the data mean), and entropy is calculated as a function of upper lengthscale. This type is displayed in **Figure 7**. In the second type, the upper lengthscale is held constant to a value equal to one average absolute deviation about the mean (AAD), and entropy is calculated as a function of the embedding window. This type is displayed in **Figure 8**.

In the entropy-lengthscale spectra, there are several important features. First, the spectra of the two lower-flow cases are distinct from the highest-flow case in both the acoustic and pressure signals. Second, the acoustic signals (**Figure 7(a)**) seem to offer better distinction between the two lower-flow cases than is seen in the pressure signals (**Figure 7(b)**). Third, entropy decreases from small (0.2 AAD) to moderate (approximately 1.5 AAD) lengthscales yet increases at much larger upper lengthscales. The lengthscale at which the normalized entropy is minimal (1.5 AAD) represents the optimal lengthscale for predictive observation based on the chosen embedding window. Fourth, entropy is lowest at the condition of maximum stable slugging and increases at other fluidization conditions because maximum stable slugging implies regularity and low entropy.

In the entropy-timescale spectra, there are several important features. First, the spectra of the two lower-flow cases are distinct from the highest-flow case in both the acoustic and pressure signals. Second, the acoustic signals (**Figure 8(a)**) seem to offer better distinction between the two lower-flow cases than is seen in the pressure signals (**Figure 8(b)**). Third, all spectra have the same general shape — entropy is high at short timescales, decreases to a minimum (at 0.8 average orbital times), and stays fairly constant for longer timescales. Where entropy first reaches the minimal value (0.8 average orbital times) represents a sufficiently long embedding window — shorter windows result in less predictability (and higher entropy) because the cycle of the sinusoidal shape of the slugging oscillations is not well-enough defined, and the nearly periodic nature of slugging, in the fluidization cases examined, means that entropy will be low for embedding windows of several average orbital times.

Fourth, entropy is lowest at the condition of maximum stable slugging and increases at other fluidization conditions.

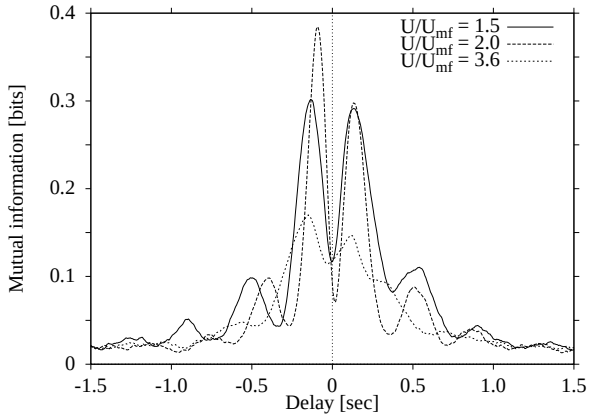

Fig. 9 Mutual information functions of acoustic-pickup with respect to pressure signal from the 15.9-cm bed at three fluidization conditions.

Figure 9 shows the mutual information functions of the acoustic with respect to simultaneously measured pressure signals for the 15.9-cm bed at the fluidization conditions. Peaks in the MIF represent timescales of strong coupling between the simultaneously measured signals. Several features are noteworthy in this figure. First, for all three fluidization conditions, the largest peaks in the MIFs occur between -0.1 and -0.2 seconds — this means that events in the acoustic signals lead or precede events in the pressure signals, as was observed in the time-series plots (**Figure 3**). Second, at long delays (> 1 second), the MIF has reached the "noise floor", meaning that on average there is little discernible predictability of the acoustic signal based on the current value of the pressure signal. Third, the signals at U/U_{mf} of 3.6 have the lowest mutual information (coupling between the acoustic and pressure signals), as might be expected based on observations of the time series. Conversely, the signals at U/U_{mf} of 2.0 have the highest degree of coupling (and mutual information), as might be expected given the visible correlation in their time-series traces.

Physically, the time lag between acoustic and pressure signals corresponds to their different sources. The large peaks in the acoustic signal represent the collapse of solids after a slug has erupted at the bed surface, whereas peaks in the pressure signal represent the subsequent compression wave as a new slug begins. The MIFs constitute a unique signature of the slugging state at each fluidization condition. The first large peak at negative lags represents the average phase difference between the signals; in the slugging regime, the location of this peak is insensitive to gas flow.

5. Conclusions

Based on observations with Group D and B particles under slugging conditions in three ambient, laboratory fluidized beds, it appears that significant information about the bed dynamics can be obtained with simple acoustic signal recording and processing. We were able to monitor slugging events by measuring and processing bed sounds to highlight the low-frequency sound-intensity modulation. This technique could prove useful for monitoring fluidized-bed systems, especially in hazardous systems where avoiding direct contact with the process is an advantage. Such monitoring capability could be used for process diagnostics (*e.g.*, the detection of agglomerates) and possibly for dynamic slugging control [24].

Acknowledgement

The authors thank Prof. Ke Nguyen and Mr. M. Vasudevan of the University of Tennessee for experimental assistance.

Nomenclature

A_{tube}	Tube cross-sectional area
A^*	Ratio of slug cross section to bed cross section
g	Acceleration of gravity
K.E.	Particle impact kinetic energy
K_{ml}	Maximum-likelihood estimator of Kolmogorov entropy
L_{slug}	Slug length
m_p	Particle mass
t_{growth}	Time for slug to grow to stable size
$t_{surface}$	Time for slug to rise to bed surface
U	Superficial gas velocity
U_{mf}	Minimum fluidization velocity
U_{mss}	Maximum stability flow
U_{slug}	Slug rise velocity
Z	Constant parameter
α	Fraction of kinetic energy converted to acoustic energy
ρ_{mf}	Solids density at minimum fluidization

Abbreviations

AAD	Average absolute deviation about the mean
AC	Alternating current
DAT	Digital audio tape
FFT	Fast Fourier transform
MIF	Mutual information function
PSD	Power spectral density function
RMS	Root mean square

References

[1] Clark, N.N., E.A. McKenzie Jr. and M. Gautam: Differential Pressure Measurements in a Slugging Fluidized Bed, Powder Technology, 67, 187–199 (1991).

[2] Clift, R. and J.R. Grace: Continuous Bubbling and Slugging, in "Fluidization", J.F. Davidson, R. Clift, and D. Harrison, eds., Academic Press, 73–132 (1985).

[3] Fan, L.S.: "Gas-Liquid-Solid Fluidization Engineering", Butterworths (1989).

[4] Geldart, D.: "Gas-Fluidization Technology", John Wiley and Sons (1986).

[5] Kühn, F.T., J.C. Schouten, R.F. Mudde, C.M. van den Bleek and B. Scarlett: Analysis of Chaos in Fluidization Using Electrical Capacitance Tomography, Meas. Sci. Technol., 7, 361–368, (1996).

[6] Yates, J.G. and S.J.R. Simons: Experimental Methods in Fluidization Research, Int. J. Multiphase Flow, 20, Suppl., 297–330 (1994).

[7] Chaouki, J., F. Larachi and M.P. Dudukovic: "Non-Invasive Monitoring of Multiphase Flows", Elsevier Science (1997).

[8] Skrzycke, D.P., K. Nguyen and C.S. Daw: Characterization of the Fluidization Behavior of Different Solid Types Based on Chaotic Time Series Analysis of Pressure Signals, Proceedings of the 12th International Conference on Fluidized Bed Combustion, 155–166 (1993).

[9] Hay, J.M., B.H. Nelson, C.L. Briens and M.A. Bergougnou: The Calculation of the Characteristics of a Chaotic Attractor in a Gas-Solid Fluidized Bed, Chem. Eng. Sci., 50, 373–380 (1995).

[10] Schouten, J.C., M.L.M. vander Stappen and C.M. van den Bleek: Scale-Up of Chaotic Fluidized Bed Hydrodynamics, Chem. Eng. Sci., 51, 1991–2000 (1996).

[11] Stappen, M.L.M. vander: "Chaotic Hydrodynamics of Fluidized Beds", Ph.D. Dissertation, Technical University of Delft (Netherlands), Delft University Press (1996).

[12] Karamavruç, A.I. and N.N. Clark: Local Differential Pressure Analysis in a Slugging Fluidized Bed Using Deterministic Chaos Theory, Chem. Eng. Sci., 52, 357–370 (1997).

[13] Cody, G.D., D.J. Goldfarb, G.V. Storch, Jr. and A.N. Norris: Particle Granular Temperature in Gas Fluidized Beds, Powder Technology, 87, 211–232 (1996).

[14] Daw, C.S., C.E.A. Finney, M. Vasudevan, N.A. van Goor, K. Nguyen, D.D. Bruns, E.J. Kostelich, C. Grebogi, E. Ott and J.A. Yorke: Self-Organization and Chaos in a Fluidized Bed, Phys. Rev. Lett., 75, 2308–2311 (1995).

[15] M'chirgui, A., H. Tadrist and L. Tadrist: Experimental Investigation of the Instabilities in a Fluidized Bed Origin of the Pressure Fluctuations, Phys. Fluids, 9, 500–509 (1997).

[16] Halow, J.S., G.E. Fasching, P. Nicoletti and J.L. Spenik: Observations of a Fluidized Bed Using Capacitance Imaging, Chem. Eng. Sci., 48, 643–659 (1992).

[17] Stappen M.L.M. vander, J.C. Schouten and C.M. van den Bleek: Deterministic chaos analysis of the dynamical behaviour of slugging and bubbling fluidized beds, Proceedings of the 12th International Conference on Fluidized Bed Combustion, 129-140 (1993).

[18] Stappen M.L.M. vander, J.C. Schouten and C.M. van den Bleek: Application of deterministic chaos theory in understanding the fluid dynamic behavior of gas-solids fluidization, AIChE Symposium Series 89:296, 91-102 (1993).

[19] Fraser, A.M. and H.L. Swinney: Independent Coordinates for Strange Attractors From Mutual Information, Phys. Rev. A, 33, 1134–1140 (1986).

[20] Daw, C.S. and J.S. Halow: Evaluation and Control of Fluidization Quality Through Chaotic Time Series Analysis of Pressure-Drop Measurements, Chemical Engineering Progress Symposium Series, American Institute of Chemical Engineers, Vol. 89, No. 286, 103–122 (1993).

[21] Karamavruç, A.I., N.N. Clark and J.S. Halow: Application of Mutual Information Theory to Fluid Bed Temperature and Differential Pressure Signal Analysis, Powder Tech., 84, 247–257 (1995).

[22] Schouten, J.C., F. Takens and C.M. van den Bleek: Maximum-Likelihood Estimation of the Entropy of an Attractor, Phys. Rev. E, 49, 126–129 (1994).

[23] Finney, C.E.A., K. Nguyen and C.S. Daw: Entropic Characterization of Cyclic Variability in Internal Combustion Engines Using Chaotic Time Series Analysis, Proceedings of the 32nd Japanese Symposium on Combustion, 400–402 (1994).

[24] Vasudevan, M., C.E.A. Finney, K. Nguyen, N.A. van Goor, D.D. Bruns and C.S. Daw: Stabilization and Destabilization of Slugging Behavior in a Laboratory Fluidized Bed, Proceedings of the 13th International Conference on Fluidized Bed Combustion, 1001–1014 (1995).

[25] Results are for two different solids over a range of bed depths and fluidization velocities: corn (23-cm bed height, 143<U<174 cm/sec; 35-cm bed height, 137<U<159 cm/sec) and millet (15-cm bed height, 65<U<95 cm/sec; 30-cm bed height, 77<U<112 cm/sec; 45-cm bed height, 68<U<138 cm/sec).

Authors's short biographies

Charles E.A. Finney

Charles Finney is a Graduate Research Assistant and Ph.D. student in mechanical engineering at the University of Tennessee, Knoxville. He received his B.A. in astronomy-physics in 1991 from the University of Virginia and B.S.M.E. in 1993 and M.S. in mechanical engineering in 1995 from the University of Tennessee. The focus of his Ph.D research is on the analysis of time-series measurements from nonlinear systems.

C. Stuart Daw

Dr. Stuart Daw is a research scientist at the Engineering Technology Division of the Oak Ridge National Laboratory. He also is Adjunct Professor of Mechanical and Chemical Engineering at the University of Tennessee, Knoxville. He received his B.S. in 1973 from the University of Florida and his M.S. in 1978 and Ph.D. in 1985 from the University of Tennessee, all with majors in chemical engineering. From 1973 to 1979, he was a R&D engineer with E.I. DuPont de Nemours in New Johnsonville, Tennessee, before joining the development staff at ORNL. His principal research interests include fluidization, chemical reactors, combustion, and nonlinear dynamics.

John S. Halow

Dr. John Halow is director of the Gaseous Fuels and Cleanup Division of the Federal Energy Technology Center in Morgantown, West Virginia. He received his B.S. in chemical engineering from Pennsylvania State University in 1964 and his Ph.D. in chemical engineering from Virginia Polytechnic Institute and State University in 1967. Prior to joining the Department of Energy, Dr. Halow was employed by Exxon Research and Engineering Company doing applied research and corporate consulting on fluid-solid systems. His principal research interests include fluidization, combustion, multi-phase flow, and nonlinear dynamics.